LETTER

doi:10.1038/nature12610

Guided hierarchical co-assembly of soft patchy nanoparticles

André H. Gröschel[1]†, Andreas Walther[2], Tina I. Löbling[1], Felix H. Schacher[3], Holger Schmalz[1] & Axel H. E. Müller[1]†

The concept of hierarchical bottom-up structuring commonly encountered in natural materials provides inspiration for the design of complex artificial materials with advanced functionalities[1,2]. Natural processes have achieved the orchestration of multicomponent systems across many length scales with very high precision[3,4], but man-made self-assemblies still face obstacles in realizing well-defined hierarchical structures[5–11]. In particle-based self-assembly, the challenge is to program symmetries and periodicities of superstructures by providing monodisperse building blocks with suitable shape anisotropy or anisotropic interaction patterns ('patches'). Irregularities in particle architecture are intolerable because they generate defects that amplify throughout the hierarchical levels. For patchy microscopic hard colloids, this challenge has been approached by using top-down methods (such as metal shading or microcontact printing), enabling molecule-like directionality during aggregation[12–16]. However, both top-down procedures and particulate systems based on molecular assembly struggle to fabricate patchy particles controllably in the desired size regime (10–100 nm). Here we introduce the co-assembly of dynamic patchy nanoparticles—that is, soft patchy nanoparticles that are intrinsically self-assembled and monodisperse—as a modular approach for producing well-ordered binary and ternary supracolloidal hierarchical assemblies. We bridge up to three hierarchical levels by guiding triblock terpolymers (length scale ~10 nm) to form soft patchy nanoparticles (20–50 nm) of different symmetries that, in combination, co-assemble into substructured, compartmentalized materials (>10 μm) with predictable and tunable nanoscale periodicities. We establish how molecular control over polymer composition programs the building block symmetries and regulates particle positioning, offering a route to well-ordered mixed mesostructures of high complexity.

Until now, research on block copolymer self-assembly in solution focused mostly on multicompartment micelles or the crystallization-driven formation of compartmentalized structures bridging one hierarchical level[17–21]. Only a few studies have considered these nanoscale superstructures to be soft colloidal building blocks (CBBs) that can be self-assembled on higher levels[22–26]. The central challenge remains to devise patchy CBBs with sufficient precision qualifying as supraparticular tectons; that is, monodisperse in size and modified with defined repulsive and attractive surface patches providing directional interaction patterns[27]. Equally problematic while operating on the nanoscale are controlled particle positioning (interparticle forces may exceed particle size), the general lack of target-oriented and predictable self-assembly protocols, and convincing visualization of nano-separated multiphase organic materials. Responsive multiblock copolymers (1–10 nm) are potential candidates for the versatile bottom-up design (geometry, patchiness and dimension) of surface-compartmentalized nanoparticles (20–50 nm) with molecular precision (Fig. 1a). The particles themselves then transmit the information needed for defined higher-level co-assembly into mesoscale structures (0.1–10 μm) of controllable size and periodicity. In contrast with 'static', patchy microparticles (hard spheres)[14,27,28], these polymer-based nanoparticles are intrinsically self-assembled, soft and 'dynamic', offering the attractive feature of assembly or disassembly on demand—from molecules to CBBs and beyond. We recently approached the design of such a system by fabricating near-monodisperse, monovalent and divalent CBBs ('monomeric units') by the self-assembly of ABC triblock terpolymers in selective solvents[23]. Shaping building-block geometries and understanding both interparticle interactions and aggregation behaviour led us to the hypothesis that the concept of soft nanoparticle self-assembly could be extended to the rational design of supracolloidal co-assemblies by suitable combinations of building blocks. Mixed particle co-assemblies across multiple hierarchical levels open a new level of complexity and have yet to be addressed.

The general design criteria—developed in an experimental approach—for the guided co-assembly of multiple CBBs with distinct valences are few and simple, and should be widely applicable to polymer-decorated

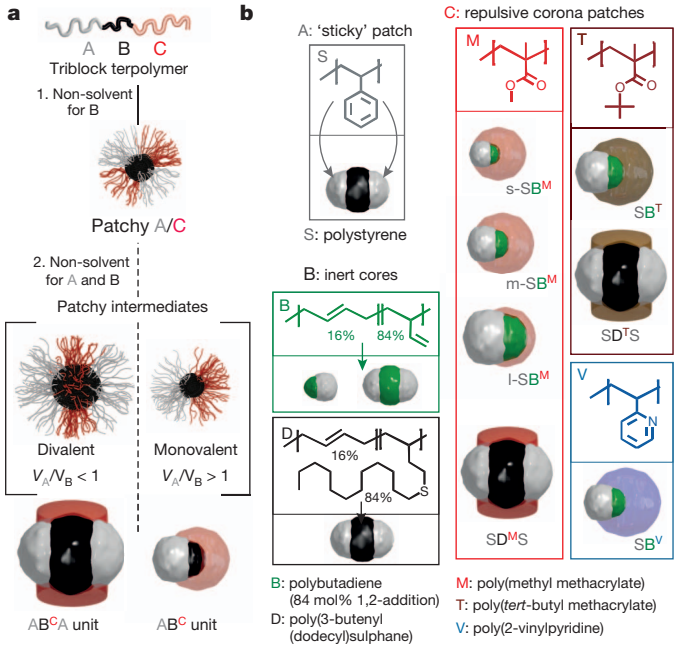

Figure 1 | Preparation and configuration of soft colloidal building blocks (CBBs). a, Dispersion of ABC triblock terpolymers in a non-solvent for B yields B-core particles with A/C corona patches. During transfer into a non-solvent for A and B, these develop into monovalent $\mathbf{AB^C}$ and divalent $\mathbf{AB^CA}$ units with sticky A patches. **b**, CBBs feature associative ('sticky') polystyrene (S) patches reversibly made solvophobic on demand, chemically different (inert) polybutadiene (B) or poly(3-butenyl(dodecyl)sulfane) (D) core material physically holding the CBBs together, and poly(methyl methacrylate) (M), poly(*tert*-butyl methacrylate) (T) or poly(2-vinylpyridine) (V) as solubilizing/repulsive corona varying in polarity and functionality.

[1]Makromolekulare Chemie II, Universität Bayreuth, D-95440 Bayreuth, Germany. [2]DWI at RWTH Aachen University, Institute for Interactive Materials Research, 52056 Aachen, Germany. [3]Institut für Organische Chemie und Makromolekulare Chemie and Jena Center for Soft Matter, Friedrich Schiller Universität Jena, D-07743 Jena, Germany. †Present addresses: Department of Applied Physics, Aalto University, FI-02150 Espoo, Finland (A.H.G.); Institute of Organic Chemistry, Johannes Gutenberg-Universität, D-55099 Mainz, Germany (A.H.E.M.).

particles (Fig. 1a). One essential requirement is tunable and defined attractive interaction patterns responsive to solvent quality or other external stimuli to favour near-monodisperse structures on different length scales. Modern polymer synthesis provides us with well-defined block copolymers with a wide range of properties and responses[29]. We developed a set of ABC triblock terpolymers into which we pre-encoded all parameters necessary for sequential, hierarchical assembly (Fig. 1b). The volume ratio of the core-forming segments, V_A/V_B, determines CBB valence, and the total molecular mass, M_n, controls particle size[23]. Thus, $V_A/V_B > 1$ yields monovalent **AB**^{C} Janus CBBs with one attractive A patch and one repulsive C patch on opposing sides of the B core (we use bold lettering to distinguish CBBs from the underlying polymer chains with regular lettering); $V_A/V_B < 1$ leads to divalent **AB**^{C}**A** with two attractive A patches on opposing sides of the B core and a repulsive C patch emanating radially from the B core. The superscript indicates that the C corona is attached to the B core (Extended Data Table 1). From here onwards we replace ABC by the actual block sequences: SBM (polystyrene-*b*-polybutadiene-*b*-poly(methyl methacrylate)) and SDM (polystyrene-*b*-poly(3-butenyl(dodecyl)sulfane)-*b*-poly(methyl methacrylate)). Monovalent **SB**^{M} and divalent **SD**^{M}**S** CBBs were prepared separately by self-assembly in *N*,*N*-dimethylacetamide (DMAc), a non-solvent for the middle blocks, B and D (Extended Data Fig. 1). At this stage the S and M patches are still soluble and not yet completely phase-separated, and they reorganize dynamically into fully developed CBBs when the S block is made insoluble. We trigger this step by changing the solvent to acetone/propan-2-ol (60:40 v/v), leading to particles with essentially different patch arrangements. **SB**^{M} and **SD**^{M}**S** thereby act as monomeric units for self-assembly and co-assembly on the next level (transmission electron microscopy (TEM) images in Fig. 2, level 1, and Extended Data Fig. 2). If kept separate, both units undergo self-assembly into spherical and linear superstructures to minimize energetically unfavourable S patch/non-solvent interfaces (Fig. 2, level 2 self-assembly), once the solvent quality has been reduced to a critical threshold for the S patches. Small corona volumes, V_M, provide less steric repulsion and promote higher aggregation numbers of **SB**^{M} units per spherical (**SB**^{M})$_x$ cluster or, similarly, higher degrees of polymerization of **SD**^{M}**S** units per [**SD**^{M}**S**]$_m$ supracolloidal polymer chain (dimer→oligomer→polymer)[23].

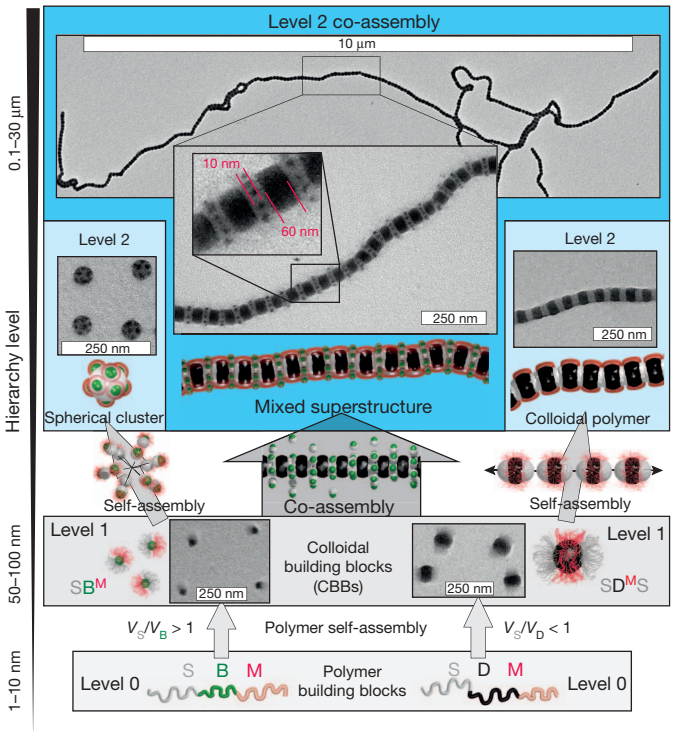

Figure 2 | Guided co-assembly across multiple hierarchical levels. Level 0: triblock terpolymers are the basic building blocks. Level 1: self-assembly of monovalent s-**SB**^{M} and divalent **SD**^{M}**S** CBBs in dependence on the volume ratios of the core-forming blocks (intermediate CBBs were captured by crosslinking; Extended Data Fig. 2). Level 2 self-assembly: s-**SB**^{M} forms spherical (**SB**^{M})$_x$ clusters and **SD**^{M}**S** linear [**SD**^{M}**S**]$_m$ supracolloidal polymer chains. Level 2 co-assembly: s-**SB**^{M} and **SD**^{M}**S** with mutually attracting S patches co-assemble into mixed superstructures stabilized by the common M corona. (OsO_4 staining: –S– segments grey, B cores dark grey, –D– segments black, and M not visible as a result of degradation by the electron beam.)

Co-assembly requires at least two CBBs differing in size (10–100 nm), patchiness or chemistry (core/corona). To demonstrate our concept, we mixed two CBBs differing in all three aspects in DMAc in defined particle ratios (s-**SB**^{M}:**SD**^{M}**S** = 8:1; Fig. 1 and Extended Data Fig. 2)[9,10] (the prefix 's' in s-**SB**^{M} stands for small). We chose small monovalent s-**SB**^{M} (hydrodynamic radius $R_h \approx 10$ nm) in combination with much larger divalent **SD**^{M}**S** ($R_h \approx 50$ nm). In DMAc, the core-forming segments (B and D) are immiscible; the two CBB species therefore do not exchange terpolymer chains and so evolve independently. As observed for individual species, changes in solvent quality for the S patch destabilize the **SD**^{M}**S** units and induce aggregation into supracolloidal polymer chains with an [**SD**^{M}**S**]$_m$ sequence. On a similar timescale, the s-**SB**^{M} units start to aggregate, yet instead of spherical clusters (self-assemblies), they selectively attach to the newly formed free surface of –S– segments within [**SD**^{M}**S**]$_m$, thereby decreasing the –S–/non-solvent interface (Fig. 2, level 2 co-assembly). In the presence of both particles we observe exclusively co-assembly under these conditions. This is surprising, because aggregation of both CBBs is driven solely by a weak non-directional force (solvophobicity) and each CBB is able to form stable populations of spherical and linear superstructures by themselves. Yet the development of [**SD**^{M}**S**]$_m$ supracolloidal polymer chains favours the attachment of s-**SB**^{M} units to the –S– segments. Therefore, we associate this phenomenon with a certain level of cooperativity. We chose s-**SB**^{M} units with a particle diameter ($d_{CBB} \approx 19$ nm) matching the width of the –S– segments of **SD**^{M}**S** ($w \approx 24$ nm) (Extended Data Fig. 2) and indeed found a defined number of seven to nine s-**SB**^{M} units radially covering the –S– segments, which perfectly reflects the original mixing ratio. On exceeding the loading capacity of the –S– segments (for example s-**SB**^{M}:**SD**^{M}**S** = 35:1), single s-**SB**^{M} CBBs or raspberry-like (s-**SB**^{M})$_x$ self-assemblies locate in the vicinity of the fully decorated co-assemblies (Extended Data Fig. 3).

Besides suitable particle ratios, the timescales of aggregation during solvent exchange have to correlate to facilitate proper co-assembly. Because the corona volume of the s-**SB**^{M} units affects the critical solvent composition needed for aggregation, we used terpolymers with different lengths of the M block (*y* stands for s (small), m (medium) or l (large) in Extended Data Table 1 and Extended Data Figs 4 and 5). Divalent **SD**^{M}**S** CBBs self-assemble under solvent conditions in which most s-**SB**$^{M(y)}$ prevail as 'monomeric' units. Stability against aggregation is best for s-**SB**$^{M(l)}$ with the largest M corona. Whereas s-**SB**$^{M(m)}$ leads to simultaneous co-assembly, s-**SB**$^{M(l)}$ shows a slight delay. However, in both cases about eight units decorate the –S– segments, pointing to a robust process with sufficient dynamics for rearrangements. However, particles with too short a corona, for example s-**SB**$^{M(s)}$, are unstable before **SD**^{M}**S** polymerization, and lateral decoration is absent. Instead, fully developed spherical (s-**SB**$^{M(s)}$)$_x$ clusters are incorporated into the linear [**SD**^{M}**S**]$_m$ superstructure during the step-growth polymerization of **SD**^{M}**S** (Extended Data Fig. 4).

The overall particle size, *x*-**SB**^{M}, of the CBBs (*x* stands for s (small), m (medium) or l (large)) markedly affects the number of particles attached to each –S– segment of the [**SD**^{M}**S**]$_m$ supracolloidal polymer chains (Fig. 3 and Extended Data Fig. 6). The particle diameter of s-**SB**^{M} units, $d_{CBB} \approx 19$ nm, allows the incorporation of eight particles on average, also slightly enlarging the width of the –S– segments from $w \approx 24$ nm to $w \approx 30$ nm (Figs 2 and 3a). Larger CBBs such as m-**SB**^{M} ($d_{CBB} \approx 35$ nm) require more space; only one particle is therefore able to attach to each –S– segment (Fig. 3b). As a result of their size and the

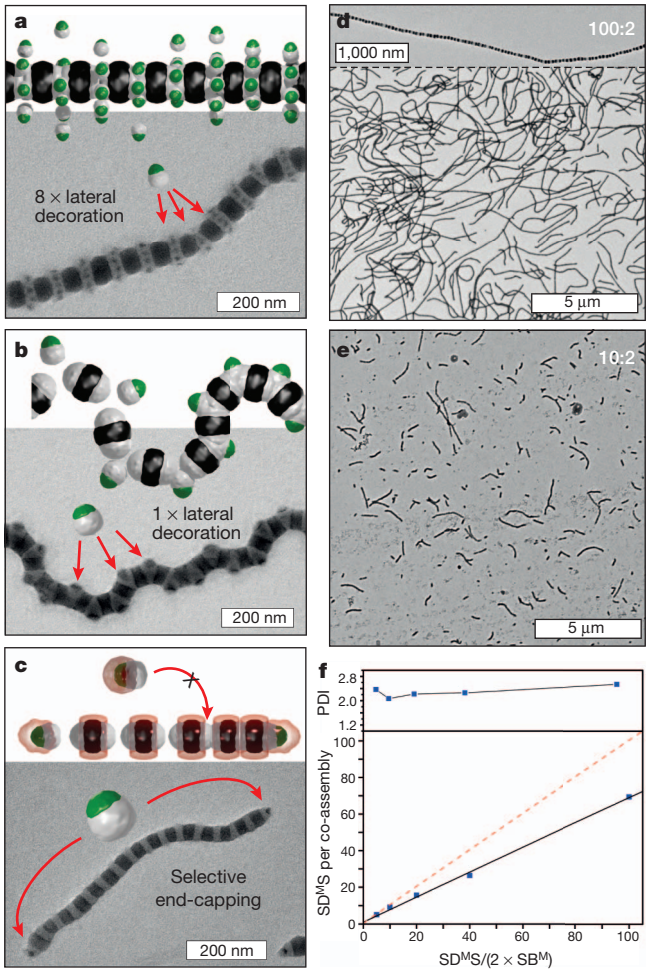

Figure 3 | Size-selective attachment and control of supracolloidal polymer chain length. **a**, The –S– segments accommodate seven to nine s-$\mathbf{SB}^{M}$ units. **b**, Larger m-$\mathbf{SB}^{M}$ units fit only once and induce strong kinks. **c**, l-$\mathbf{SB}^{M}$ units are too large for lateral decoration and instead act as selective end-cappers. **d**, **e**, Length control of supracolloidal polymer chains by the mixing of 100 (**d**) and 10 (**e**) $\mathbf{SD}^{M}\mathbf{S}$ units per two l-$\mathbf{SB}^{M}$ end-cappers (Extended Data Fig. 7). Inset shows $[\mathbf{SD}^{M}\mathbf{S}]_m$ nanostructure. **f**, Polydispersity indices (PDI; top) and linear dependence of $\mathbf{SD}^{M}\mathbf{S}$ repeating units on the mixing ratio (bottom).

accompanied volume displacement inside the –S– segments, m-$\mathbf{SB}^{M}$ units induce strong kinks altering the flexibility and linearity of the co-assembly, which could potentially influence the rheological characteristics and colloidal chain packing. l-$\mathbf{SB}^{M}$ and units substantially exceeding the width of the –S– segments ($d_{CBB} \approx 47$ nm) are too large for lateral decoration and specifically locate on terminal positions (Fig. 3c). The relative sizes of the monovalent units and the –S– segment of the divalent units govern the location and loading capacity, whereas the size of the stabilizing M patch determines the timescales and extent of co-assembly.

Selective end-capping provides an attractive handle to control the length of the $[\mathbf{SD}^{M}\mathbf{S}]_m$ supracolloidal polymer chains. Adding l-$\mathbf{SB}^{M}$ 'stoppers' in specific ratios also allows end-functionalization with chemically different CBBs. Without any end-capper, the $\mathbf{SD}^{M}\mathbf{S}$ units grow into extended structures in the region of 30 µm long (more than 600 repeating units; Extended Data Fig. 7), reaching scales visible by optical microscopy (Extended Data Fig. 6). Figure 3d–f summarizes the dependence of the length distribution of the co-assemblies on the mixing ratio $\mathbf{SD}^{M}\mathbf{S}$:l-$\mathbf{SB}^{M}$ (Extended Data Fig. 7). The decrease in mean length is evident when comparing the TEM images in Fig. 3d, e, which show mixing ratios of 100:2 and 10:2. Stoichiometric control as known from step-growth polymerizations is corroborated by the linear dependence of the average degree of polymerization on the mixing ratio (Fig. 3f). The deviation from the theoretical values (dashed line) is caused by residual 'defects' in the CBBs, because we find a small proportion (less than 1%) of trivalent $\mathbf{S_3D}^{M}$ CBBs that induce branching. Matching patch sizes of CBBs and low corona volumes of the $\mathbf{SB}^{M}$ units are decisive in efficient end-capping: the first effectively prevents the addition of $\mathbf{SD}^{M}\mathbf{S}$ monomeric units and the latter causes the $\mathbf{SB}^{M}$ units to interfere directly with $\mathbf{SD}^{M}\mathbf{S}$ polymerization. Both factors can be programmed molecularly into the $\mathbf{SB}^{M}$ units by variation of the total molecular mass (particle size) and the fraction of M (onset of aggregation).

Controlled mixing of different CBBs permits the rational design and precise implementation of functionalities within the core and/or corona of the co-assemblies (Fig. 4). We prepare hybrid materials by selectively encapsulating 10-nm maghemite nanoparticles within the –D– segments of $\mathbf{SD}^{M}\mathbf{S}$ CBBs on hierarchy level 1 (Fig. 4a). Selective and reversible loading yields a unique advantage compared with top-down approaches that require the synthesis of tailored colloids. The preloaded CBBs then polymerize further to linear chains with alternating D-loaded/S-empty compartments. Nanoparticles with tailored affinities for other phases may allow the preparation of bar-coded distributions, and magnetically responsive co-assemblies may serve as advanced viscosity modifiers or may act as deterministic carrier systems. We also generated co-assemblies comprising five different environments (three core/two corona compartments; Fig. 4b) by mixing $\mathbf{SD}^{M}\mathbf{S}$ with $\mathbf{SB}^{T}$ (T = poly(*t*-butyl methacrylate)), which leads to the already established $[\mathbf{SD}^{M}\mathbf{S}]_m$ core sequence, yet now with a segmented M/T corona. In principle, such structures allow us to control the positioning of nanoparticles along the co-assemblies or to implement predefined responsive folding sites. At this point we emphasize enhanced superstructure stability, because the pristine $[\mathbf{SD}^{M}\mathbf{S}]_m$ immediately precipitates in ethanol (non-solvent for M) and the $\mathbf{SB}^{T}$/$[\mathbf{SD}^{M}\mathbf{S}]_m$ co-assemblies remain stable (Extended Data Fig. 8).

We extended this approach and designed multiblock co-assemblies by combining two divalent units, $\mathbf{SD}^{M}\mathbf{S}$ and $\mathbf{SB}^{M}\mathbf{S}$ (Fig. 4c). Here, several short segments of $[\mathbf{SD}^{M}\mathbf{S}]_m$ or $[\mathbf{SB}^{M}\mathbf{S}]_n$ sequences are coupled into multiblock co-assemblies. We suggest that the homogeneity and sequence distribution depend on how synchronized self-assembly and co-assembly occur and that deeper kinetic studies will eventually enable control over the sequence length. In an analogy with polymer architectures, we fabricated telechelic oligomers with terminal functional groups by end-capping $[\mathbf{SD}^{M}\mathbf{S}]_{10}$ oligomers with $\mathbf{SB}^{V}$ (V = poly(2-vinylpyridine); Fig. 4d). The number-average length of the telechelics scales with the mixing ratio $\mathbf{SD}^{M}\mathbf{S}$:$\mathbf{SB}^{V}$. The V corona is clearly visible as grey end-cap by TEM (Fig. 4d, central inset). Protonation of the V corona with HCl causes solvophobic attraction and triggers aggregation of the V-termini into extended subdivided superstructures. We emphasize that this process is fully reversible and that it corresponds to a step-growth polymerization on two levels: first for the individual $\mathbf{SD}^{M}\mathbf{S}$ units, and then chain extension of the telomerized 'macromonomers'. Combining selective end-capping and lateral decoration yields ternary structures. The addition of $\mathbf{SB}^{M}$ units to the $\mathbf{SB}^{V}$-$[\mathbf{SD}^{M}\mathbf{S}]_{10}$-$\mathbf{SB}^{V}$ telechelic oligomers does indeed lead to the decoration of the –S– segments and a final composition of $\mathbf{SB}^{M}$:$\mathbf{SD}^{M}\mathbf{S}$:$\mathbf{SB}^{V}$ = 10:10:2.

Finally, we bridge three hierarchical levels by co-assembly of $\mathbf{SB}^{M}$ and $\mathbf{SD}^{T}\mathbf{S}$ building blocks into end-capped colloidal molecules with the composition $(\mathbf{SB}^{M})_N$-$[\mathbf{SD}^{T}\mathbf{S}]_1$-$(\mathbf{SB}^{M})_N$ (where the number of end-caps N = 1–5). The CBB mixing ratio determines the number of end-cappers; for example, $\mathbf{SB}^{M}$:$\mathbf{SD}^{T}\mathbf{S}$ = 2:1 gives $(\mathbf{SB}^{M})_1$-$[\mathbf{SD}^{T}\mathbf{S}]_1$-$(\mathbf{SB}^{M})_1$. These co-assemblies self-assemble spontaneously into triangles and further into two-dimensional networks when cast onto substrates, a necessary two-dimensional confinement tool[13,30], and the number of end-caps ($\mathbf{SB}^{M}$) directs the number of nearest neighbours at the network linkages (Fig. 4e). The self-assembly of these colloidal molecules is directed by the M/T corona patches that change their volume on solvent evaporation and develop into attractive M and repelling T patches. For N = 1 or 2 the end-cap size allows three or four nearest

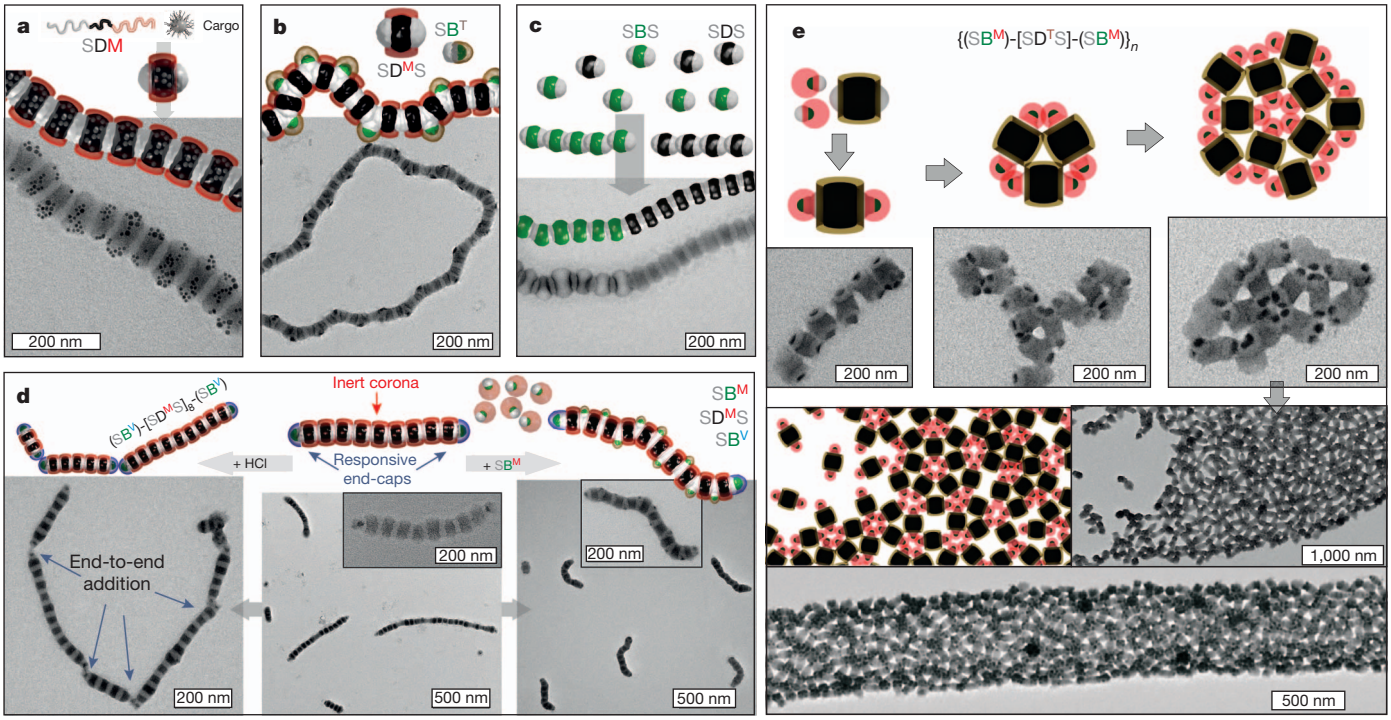

Figure 4 | Binary and ternary co-assemblies. **a**, Hybrid co-assemblies with magnetite nanoparticles selectively loaded into one core segment. **b**, Core and corona co-assemblies. The $[\mathbf{SD^MS}]_m$ superstructure is decorated with $\mathbf{SB^T}$ CBBs, yielding an alternating M/T corona. **c**, Linear multiblock co-assembly composed of $[\mathbf{SD^MS}]_m/[\mathbf{SB^MS}]_n$ sequences (M corona omitted for clarity). **d**, $\mathbf{SB^V}$ end-cappers produce telechelic $[\mathbf{SD^MS}]_{10}$ oligomers (grey V corona surrounding the $\mathbf{SB^V}$ end-cap in inset). Protonation with HCl triggers further polymerization, and decoration with $\mathbf{SB^M}$ units yields ternary co-assemblies. **e**, Multicomponent structuring across three hierarchical levels. In solution, the terpolymers self-assemble into CBBs that co-assemble into colloidal molecules; these finally self-assemble into networks after drop-casting on a substrate.

neighbours, $\{\mathbf{SB^M}\text{-}\mathbf{SD^TS}\text{-}\mathbf{SB^M}\}_{4,5}$, whereas for $N = 3$–5 there is only space for two nearest neighbours and the networks show the onset of distorted kagome lattice formation (Extended Data Fig. 9).

These hierarchical multicomponent superstructures demonstrate the level of complexity reached through the controlled co-assembly of soft patchy nanoparticles and is in stark contrast to the self-assembly of increasingly complex building blocks (shape and surface pattern). Using proper interacting segments, a wide range of building block combinations is conceivable, from biological origin to inorganic and organic nanoparticles and microparticles. Various self-assembly stimuli can conveniently be implemented by means of functional polymer blocks, for example supramolecular interactions, chemical reactions and environmental triggers (solvent polarity, pH, temperature, light or electrochemistry). Co-assembly opens up avenues to construct new materials, also far from thermodynamic equilibrium, through the tailored spatial organization of functionalities and the control of kinetics. We foresee application possibilities in smart materials, sensing, photonics and nanolithography.

METHODS SUMMARY

Relevant parameters of SBM, SBV and SBT triblock terpolymers are summarized in Fig. 1 and Extended Data Table 1. SBM and SBT were converted to SDM and SDT by thiol-ene click reaction of 1-dodecane thiol to the poly(1,2-butadiene) block. All CBBs were prepared in DMAc at a polymer concentration of 0.1 g l^{-1} and annealed overnight at 70 °C. Particle dispersions were mixed in specific particle ratios and 10 ml of solution was co-dialysed (molecular mass cut-off 12,000–14,000 g mol^{-1}; Roth) against 5 l of selective solvent or solvent mixture for the corona block (acetone/propan-2-ol for M and V; ethanol for T corona). The solvent exchange was monitored by ^{1}H-NMR. TEM was performed in bright-field mode on Zeiss CEM 902 and 922 OMEGA electron microscopes operated at 80 kV and 200 kV, respectively. Co-assemblies were deposited by drop-casting (0.05 ml of 0.1 mg ml^{-1} dispersion) onto carbon-coated copper grids resting on a filter paper to blot excess solution immediately. Samples were exposed to OsO_4 vapour for 2 h to stain the polybutadiene blocks selectively.

Online Content Any additional Methods, Extended Data display items and Source Data are available in the online version of the paper; references unique to these sections appear only in the online paper.

Received 26 March; accepted 28 August 2013.
Published online 3 November 2013.

1. Whitesides, G. M. & Grzybowski, B. Self-assembly at all scales. *Science* **295,** 2418–2421 (2002).
2. Studart, A. R. Towards high-performance bioinspired composites. *Adv. Mater.* **24,** 5024–5044 (2012).
3. Fratzl, P. & Weinkammer, R. Nature's hierarchical materials. *Prog. Polym. Sci.* **52,** 1263–1334 (2007).
4. Mann, S. Self-assembly and transformation of hybrid nano-objects and nanostructures under equilibrium and non-equilibrium conditions. *Nature Mater.* **8,** 781–792 (2009).
5. Glotzer, S. C. & Solomon, M. J. Anisotropy of building blocks and their assembly into complex structures. *Nature Mater.* **6,** 557–562 (2007).
6. Quan, Z. & Fang, J. Superlattices with non-spherical building blocks. *Nano Today* **5,** 390–411 (2010).
7. Wang, T. *et al.* Self-assembled colloidal superparticles from nanorods. *Science* **338,** 358–363 (2012).
8. Grzelczak, M., Vermant, J., Furst, E. M. & Liz-Marzán, L. M. Directed self-assembly of nanoparticles. *ACS Nano* **4,** 3591–3605 (2010).
9. Nie, Z. *et al.* Self-assembly of metal-polymer analogues of amphiphilic triblock copolymers. *Nature Mater.* **6,** 609–614 (2007).
10. Liu, K. *et al.* Step-growth polymerization of inorganic nanoparticles. *Science* **329,** 197–200 (2010).
11. Cui, H., Chen, Z., Zhong, S., Wooley, K. L. & Pochan, D. J. Block copolymer assembly via kinetic control. *Science* **317,** 647–650 (2007).
12. Chen, Q. *et al.* Supracolloidal reaction kinetics of Janus spheres. *Science* **331,** 199–202 (2011).
13. Chen, Q., Bae, S. C. & Granick, S. Directed self-assembly of a colloidal kagome lattice. *Nature* **469,** 381–384 (2011).
14. Wang, Y. *et al.* Colloids with valence and specific directional bonding. *Nature* **491,** 51–55 (2012).
15. Kaufmann, T. *et al.* 'Sandwich' microcontact printing as a mild route towards monodisperse Janus particles with tailored bifunctionality. *Adv. Mater.* **23,** 79–83 (2010).
16. Chen, Q., Bae, S. C. & Granick, S. Staged self-assembly of colloidal metastructures. *J. Am. Chem. Soc.* **134,** 11080–11083 (2012).
17. Li, Z., Kesselman, E., Talmon, Y., Hillmyer, M. A. & Lodge, T. P. Multicompartment micelles from ABC miktoarm stars in water. *Science* **306,** 98–101 (2004).

18. Wang, X. *et al.* Cylindrical block copolymer micelles and co-micelles of controlled length and architecture. *Science* **317,** 644–647 (2007).
19. Schmelz, J., Schedl, A. E., Steinlein, C., Manners, I. & Schmalz, H. Length control and block-type architectures in worm-like micelles with polyethylene cores. *J. Am. Chem. Soc.* **134,** 14217–14225 (2012).
20. Gädt, T., Ieong, N. S., Cambridge, G., Winnik, M. A. & Manners, I. Complex and hierarchical micelle architectures from diblock copolymers using living, crystallization-driven polymerizations. *Nature Mater.* **8,** 144–150 (2009).
21. Kubowicz, S. *et al.* Multicompartment micelles formed by self-assembly of linear ABC triblock copolymers in aqueous medium. *Angew. Chem. Int. Ed.* **44,** 5262–5265 (2005).
22. Gröschel, A. H. *et al.* Facile, solution-based synthesis of soft, nanoscale Janus particles with tunable Janus balance. *J. Am. Chem. Soc.* **134,** 13850–13860 (2012).
23. Gröschel, A. H. *et al.* Precise hierarchical self-assembly of multicompartment micelles. *Nature Commun.* **3,** 710, http://dx.doi.org/10.1038/ncomms1707 (2012).
24. Li, Z., Hillmyer, M. A. & Lodge, T. P. Control of structure in multicompartment micelles by blending μ-ABC star terpolymers with AB diblock copolymers. *Macromolecules* **39,** 765–771 (2005).
25. Fang, B. *et al.* Undulated multicompartment cylinders by the controlled and directed stacking of polymer micelles with a compartmentalized corona. *Angew. Chem. Int. Ed.* **48,** 2877–2880 (2009).
26. Rupar, P. A., Chabanne, L., Winnik, M. A. & Manners, I. Non-centrosymmetric cylindrical micelles by unidirectional growth. *Science* **337,** 559–562 (2012).
27. Chen, Q., Yan, J., Zhang, J., Bae, S. C. & Granick, S. Janus and multiblock colloidal particles. *Langmuir* **28,** 13555–13561 (2012).
28. Sacanna, S., Irvine, W. T. M., Chaikin, P. M. & Pine, D. J. Lock and key colloids. *Nature* **464,** 575–578 (2010).
29. Bates, F. S. *et al.* Multiblock polymers: panacea or Pandora's box? *Science* **336,** 434–440 (2012).
30. Bowden, N., Terfort, A., Carbeck, J. & Whitesides, G. M. Self-assembly of mesoscale objects into ordered two-dimensional arrays. *Science* **276,** 233–235 (1997).

Acknowledgements We thank O. Ikkala and E. Kumacheva for discussions and comments on the manuscript, and A. Majewski for providing maghemite nanoparticles. This work was supported by Deutsche Forschungsgemeinschaft within Sonderforschungsbereich 840 (TP A1 and A2).

Author Contributions A.H.G. initiated the project. A.H.G. and T.I.L. performed experiments and collected data. A.H.G., A.W. and A.H.E.M. designed the experiments, discussed results and wrote the manuscript. F.H.S. co-designed experiments, discussed results and commented on the manuscript. H.S. provided polymers, discussed results and commented on the manuscript. A.H.E.M. supervised the project.

Author Information Reprints and permissions information is available at www.nature.com/reprints. The authors declare no competing financial interests. Readers are welcome to comment on the online version of the paper. Correspondence and requests for materials should be addressed to A.H.E.M. (axel.mueller@uni-mainz.de) or A.H.G. (andre.groschel@aalto.fi).

METHODS

Particle preparation. All terpolymers were synthesized by sequential anionic polymerization[31–35]. Important parameters are summarized in Fig. 1 and Extended Data Tables 1. All solvents used were of analytical grade. Dialysis tubes of regenerated cellulose with a molecular mass cut-off of 12,000–14,000 g mol^{-1} were purchased from Roth. Oleic acid-stabilized maghemite nanoparticles were synthesized as described elsewhere[36]. Both polymers, SBM and SBT, were converted to SDM and SDT, respectively, by means of a thiol-ene click reaction of 1-dodecane thiol with the pendant double bonds of poly(1,2-butadiene). In a typical experiment, terpolymer (0.5 g) was dissolved in 20 ml of tetrahydrofuran; 20 ml of 1-dodecane thiol were added and the solution was purged for 15 min with argon. The mixture was irradiated for 24 h with an ultraviolet lamp with a cut-off filter ($\lambda = 300$ nm; $\lambda_{max} = 360$ nm). After the reaction, the modified terpolymer was precipitated in propan-2-ol, filtered, and washed with excess propan-2-ol to remove remaining 1-dodecane thiol. SBM, SDM, SBT, SDT and SBV triblock terpolymers were dissolved separately in DMAc at an initial polymer concentration of 0.1 g l^{-1} and annealed overnight at 70 °C to guarantee an equilibrated system. At this stage of self-assembly the corona patches were not yet fully developed. To reveal the patches in the developed state (Extended Data Fig. 2), the CBBs were crosslinked while located within the respective superstructure. Therefore, 2 equivalents of the photo-crosslinker 2,4,6-trimethylbenzoyldiphenylphosphineoxide (Lucirin TPO; $\lambda_{max} \approx 360$ nm), were added to each double bond. Gentle stirring for 2 h ensured a homogeneous distribution of the photo-crosslinker before the samples were irradiated for 1 h with an ultraviolet lamp with a cut-off filter ($\lambda = 300$ nm). Redispersion in DMAc as a good solvent for the patches then broke up the superstructures into the respective CBBs.

Self-assembly and co-assembly. CBB solutions (0.1 g l^{-1} in DMAc) were mixed in specific particle ratios to yield 10 ml of a colloidal mixture and co-dialysed against 5 l of selective solvent/solvent mixture for the corona block (acetone/propan-2-ol for the M corona and V corona block, and ethanol for the T-corona block). The solvent exchange was monitored by ^{1}H-NMR. TEM was performed in bright-field mode on Zeiss CEM 902 and LEO 922 OMEGA electron microscopes operated at 80 kV and 200 kV, respectively. Samples were prepared by dropping 0.05 ml of a 0.1 mg ml^{-1} colloidal suspension onto carbon coated copper grids resting on a filter paper to remove the excess solution immediately. The two-dimensional networks were prepared similarly, except from 0.01 g l^{-1} colloidal suspension that was allowed to settle on the TEM grid for 30 s before blotting. TEM grids were then exposed for 2 h to OsO_4 vapour to stain the polybutadiene block selectively. The number of polymer chains in each CBB was determined, evaluating at least 250 cores. The average degree of polymerization of each [**SD^{M}S**]$_m$ colloidal polymer was determined by counting the black segments of 500 colloidal polymers and plotted as frequency distribution.

Correlating co-assembly with onsets of aggregation. We used a CBB ratio of s-**SB**$^{M(y)}$:**SD^{M}S** = 8:1 for all experiments to ensure that enough monovalent CBBs were present for full decoration of the –S– segments. **SD^{M}S** was co-dialysed with three different s-**SB**$^{M(y)}$ units with varying volume of the corona, M(y) (y stands for s (small), m (medium) or l (large)). The dialysis sequence was from DMAc into acetone/propan-2-ol mixtures. Greater amounts of propan-2-ol led to a contraction of the M corona. **SD^{M}S** forms extended superstructures irrespective of the propan-2-ol content (also in pure acetone). s-**SB**$^{M(l)}$ CBBs with a large relative volume fraction of the soluble M corona of $r_M = 0.74$ (where $r_M = V_M/(V_S + V_B)$) do not co-assemble at low propan-2-ol contents (less than 20 vol%) and are only located in the vicinity of polymerized **SD^{M}S** (Extended Data Fig. 4). The long corona blocks provide steric stabilization by fully covering the CBB. At high propan-2-ol contents (30 vol%), partial co-assembly is observed and quantitative co-assembly only at 40 vol% as a result of progressive contraction of the M corona. Because the **SD^{M}S** units are already fully polymerized, decoration does not interfere with the growth process (no premature end-capping). s-**SB**$^{M(m)}$ CBBs with $r_M = 0.34$ carry a corona block of moderate length and show partial to quantitative co-assembly over the whole range of solvent mixtures, indicating only a slight difference in onset of aggregation between **SD^{M}S** and s-**SB**$^{M(m)}$. s-**SB**$^{M(s)}$ CBBs with the shortest corona block, $r_M = 0.15$, show no co-assembly in either of the solvent compositions: at a propan-2-ol content of only 10 vol% the corona shows insufficient stabilization for the s-**SB**$^{M(s)}$ CBBs, and aggregation into spherical (s-**SB**$^{M(s)}$)$_x$ clusters occurs before polymerization of **SD^{M}S**. The **SD^{M}S** units still polymerize through these spherical clusters, resulting in randomly distributed bulbs of (s-**SB**$^{M(s)}$)$_x$ clusters along the [**SD^{M}S**]$_n$ chain.

Calculation of polymer chains in each particle and compartment volumes. Because CBBs form dynamically during the self-assembly of triblock terpolymers, one needs to know how many polymer chains are located within one CBB to be able to mix CBBs in the desired ratios for the co-assembly process. We determined the average core diameter of each CBB by TEM (averaged over 250 samples) to calculate the aggregation number of triblock terpolymer chains, N_{agg}, in each CBB. This evaluation is exemplified on monovalent spherical s-**SB^M** and divalent, cylindrical **SD^{M}S** cores (Extended Data Fig. 2). N_{agg} was then calculated from

$$N_{agg} = \frac{m_{core}}{m_B^{chain}} = V_{core}\frac{N_A \rho_B}{M_B^{chain}}$$

with $V_{core} = 4/3(\pi R_{core}^3)$ for spherical **SB^M** and $V_{core} = w\pi R_{core}^2$ for cylindrical **SD^{M}S**; m_{core} is the mass of the micellar core, m_B^{chain} is the mass of the middle block, M_B^{chain} is the molecular mass of the middle block, N_A is Avogadro's constant and ρ_B is the density of the middle block. We found that this approach yields a good correlation between the ratio of triblock terpolymers and the final composition of CBBs in the co-assemblies. We can calculate the diameter of **SB^M** units combining the calculated volume for the B compartments, V_B, from N_{agg} with the volume ratio V_S/V_B. The diameter of spherical CBBs, d_{CBB}, is then given by

$$d_{CBB} = 2\left(\left(V_S + \frac{1}{2}V_B\right)\frac{3}{4\pi}\right)^{\frac{1}{3}}$$

The volume and surface area of the cylindrical –S– segments are simply determined from TEM data; that is, directly from the colloidal co-assembly as width (w) and height = diameter (d).

31. Auschra, C. & Stadler, R. Synthesis of block copolymers with poly(methyl methacrylate): P(B-*b*-MMA), P(EB-*b*-MMA), P(S-*b*-B-*b*-MMA) and P(S-*b*-EB-*b*-MMA). *Polym. Bull.* **30,** 257–264 (1993).
32. Giebeler, E. & Stadler, R. ABC triblock polyampholytes containing a neutral hydrophobic block, a polyacid and a polybase. *Macromol. Chem. Phys.* **198,** 3815–3825 (1997).
33. Walther, A., André, X., Drechsler, M., Abetz, V. & Müller, A. H. E. Janus discs. *J. Am. Chem. Soc.* **129,** 6187–6198 (2007).
34. Schacher, F., Yuan, J., Schoberth, H. G. & Müller, A. H. E. Synthesis, characterization, and bulk crosslinking of polybutadiene-*block*-poly(2-vinyl pyridine)-*block*-poly(*tert*-butyl methacrylate) block terpolymers. *Polymer* **51,** 2021–2032 (2010).
35. Ruckdäschel, H. *et al.* Compatibilisation of PPE/SAN blends by triblock terpolymers: correlation between block terpolymer composition, morphology and properties. *Polymer* **47,** 2772–2790 (2006).
36. Majewski, A. P. *et al.* Dual-responsive magnetic core–shell nanoparticles for nonviral gene delivery and cell separation. *Biomacromolecules* **13,** 857–866 (2012).

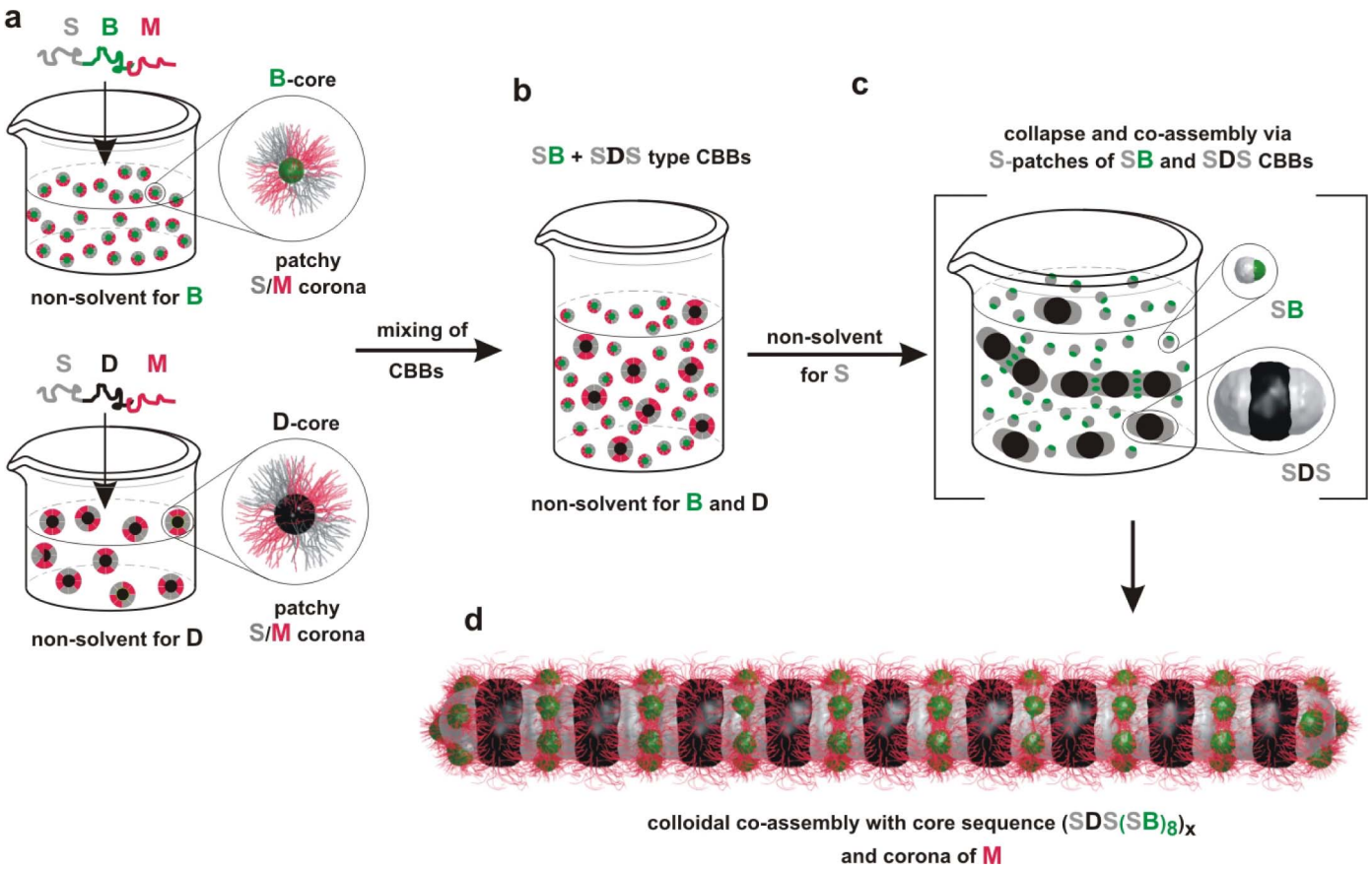

Extended Data Figure 1 | Experimental approach to prepare colloidal co-assemblies exemplified on s-SB^{M} and SD^{M}S. a, First, the triblock terpolymers are dispersed separately in DMAc as a non-solvent for B and D, equalling bottom-up structuring of CBBs with different cores (B and D), yet identical 'sticky' S patch and stabilizing M corona. **b**, Both colloidal dispersions are mixed in specific ratios and stirred overnight to ensure homogeneous distribution. **c**, Co-dialysis into a non-solvent for the S patches induces collapse and aggregation. **SD^{M}S** grows into extended linear colloidal polymers decorated by s-**SB^{M}** units (M corona omitted for clarity). **d**, Final colloidal co-assemblies stabilized by the common M corona.

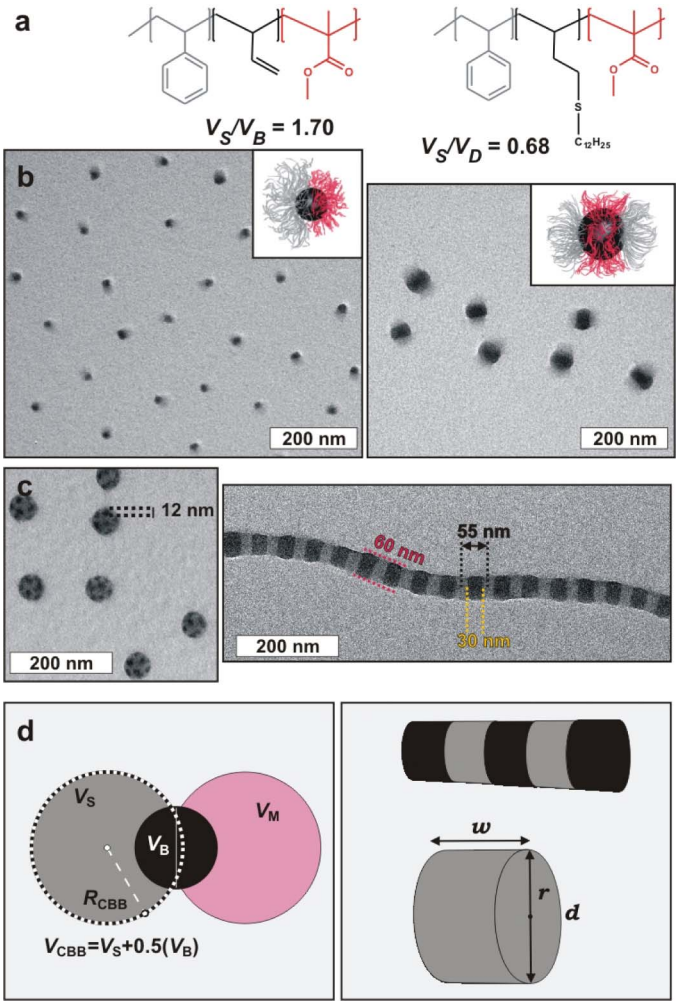

Extended Data Figure 2 | Compartment sizes, polymer chains per CBB and CBB mixing ratios. **a**, SBM with $V_S/V_B = 1.70$ and SDM with $V_S/V_D = 0.68$ result in **b,** monovalent **SB**^{M} (Janus) and divalent **SD**^{M}**S** units, respectively. CBBs are visualized after crosslinking of the remaining double bonds within the particle cores. **c**, Examples of spherical **SB**^{M} clusters and linear **SD**^{M}**S** colloidal polymers. **d**, Diagrams of CBB compartment volumes and surface area of associative patches. We determine the number of **SB**^{M} units able to attach to the –S– segments of the **SD**^{M}**S** colloidal polymers by calculating the volume and the diameter of the CBBs, assuming a spherical shape of B and S phases and considering the number of polymer chains per patch. The spherical **SB**^{M} units are composed of (i) the body as the sum of the collapsed S patch (grey) and B core (black) and (ii) the M corona patch. The radius, R_{CBB}, and the volume, V_{CBB}, displaced by the CBB when aggregating into the –S– segments are estimated by combining the volume of S plus half of the volume of B (the dashed line marks R_{CBB}). These assumptions are valid for the collapsed state, given the unfavourable interactions with the surrounding medium and the minimization of the interfacial energies.

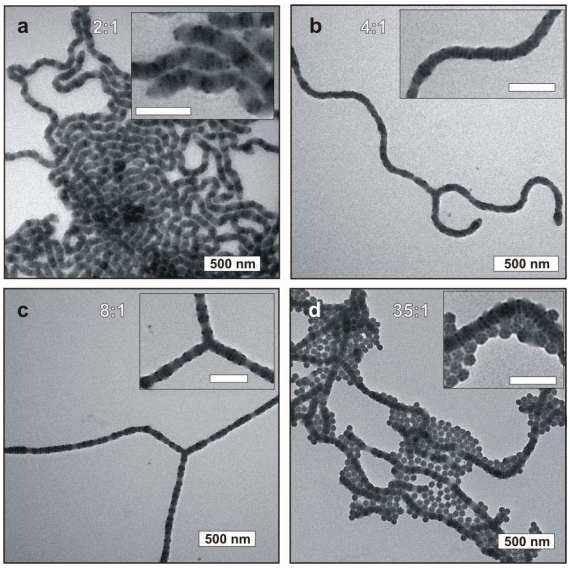

Extended Data Figure 3 | Loading capacity for decoration with spherical CBBs during co-assembly. **SD^{M}S** and s-**SB**^{M} colloidal co-assemblies with increasing mixing ratios 2:1, 4:1, 8:1 and 35:1 of s-**SB**^{M}:**SD**^{M}**S** and corresponding co-assembly composition. **a**, At small excess, s-**SB**^{M}:**SD**^{M}**S** = 2:1, the –S– segments are only partly decorated. **b**, **c**, With increasing CBB ratio, the –S– segments of the colloidal polymers are more strongly occupied (4:1) (**b**) and at full capacity in a radial manner (8:1) (**c**). **d**, Above this ratio, no space remains on the colloidal polymer and only then does s-**SB**^{M} start to form homo-clusters (35:1; football-like or raspberry-like homo-clusters adjacent to the colloidal co-assemblies). These observations fit well with our calculations, as a cylinder with $d_{\text{-S-}} \approx 55$ nm and $w \approx 24$ nm can accommodate up to nine s-**SB**^{M} units with $d_{\text{CBB}} \approx 19$ nm ($\pi d_{\text{-s-}} \approx 173$ nm; 173 nm/19 nm ≈ 9.1). Scale bars in insets are 200 nm (OsO_4 staining: S grey, B dark grey dots, D black, and M not visible as a result of degradation by the electron beam.)

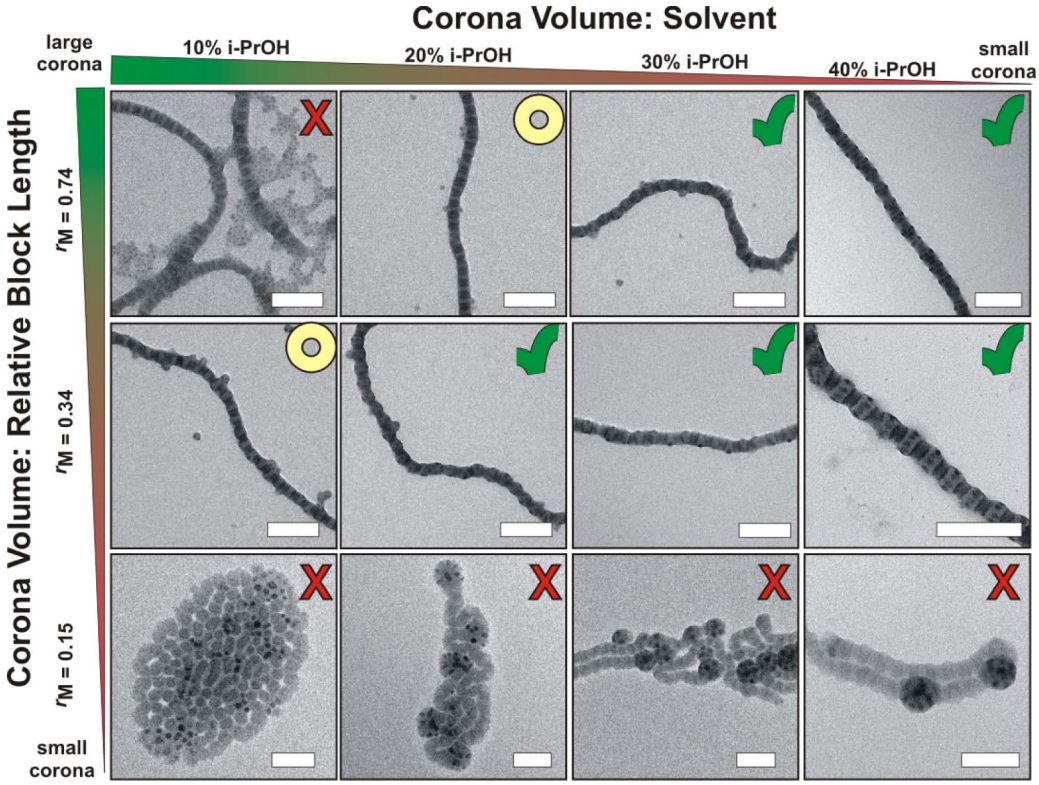

Extended Data Figure 4 | Co-assembly of s-SB$^{M(y)}$ and SD^{M}S in dependence on the corona volume of the monovalent s-SB$^{M(y)}$ units (*y* stands for s, m or l). Colloidal co-assembly occurs preferentially with matching onsets of aggregation that depend on the corona volume, which is tunable either by decreasing the block length of the corona block, $r_M = V_M/(V_S + V_B)$, r_M(s-**SB**$^{M(l)}$) = 0.74, r_M(s-**SB**$^{M(m)}$) = 0.34, r_M(s-**SB**$^{M(s)}$) = 0.15, or by reducing the solvent quality, here the addition of propan-2-ol from 10 vol% to 40 vol%. Thereby, crosses indicate no co-assembly, circles the onset of co-assembly and tick marks effective and quantitative co-assembly. For detailed discussion see Methods. (OsO_4 staining: S grey, B dark grey dots, D black, and M not visible as a result of degradation by the electron beam.)

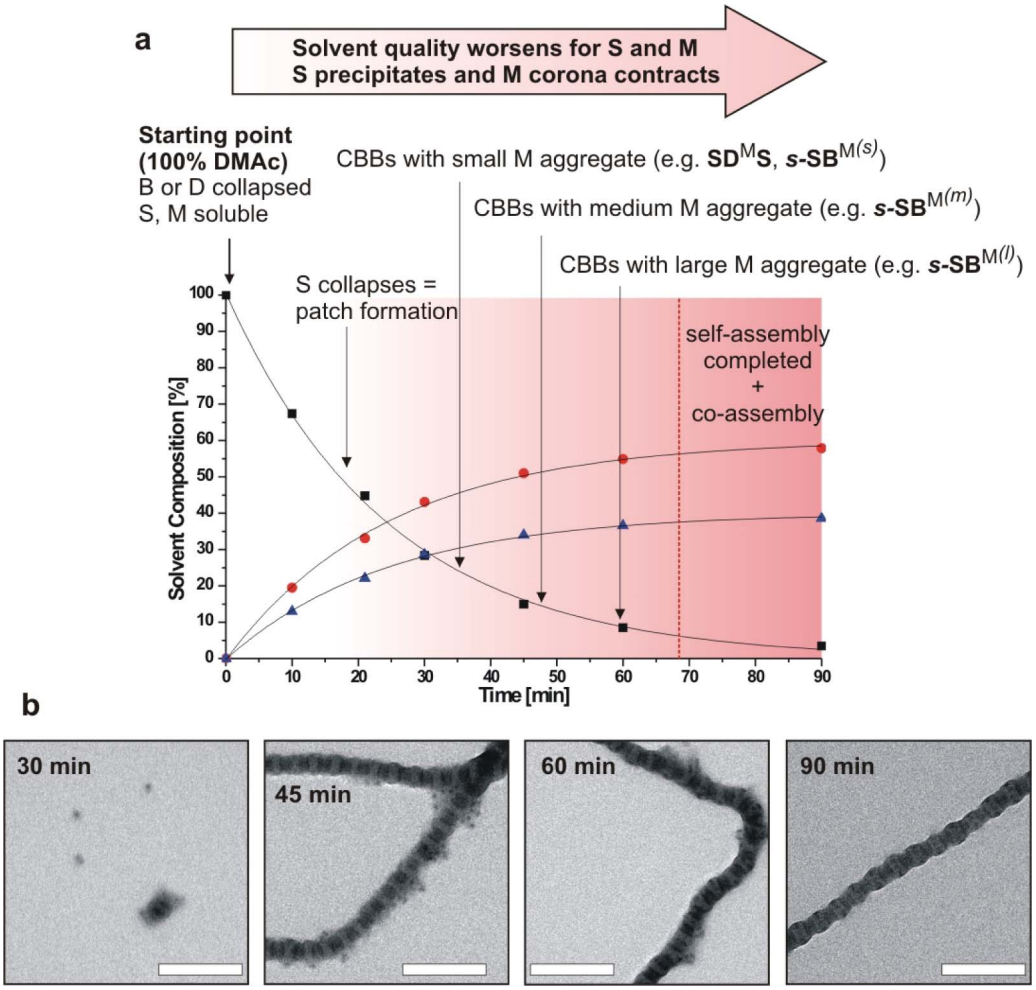

Extended Data Figure 5 | Timeline of CBB aggregation and response of CBB constituents on solvent composition. **a**, Co-dialysis of CBBs (here **SD**^{M}**S** and s-**SB**$^{M(y)}$) from DMAc (squares) into acetone (circles)/propan-2-ol (triangles) mixtures (60:40 v/v) results in a continuous change of a multitude of polymer–polymer interactions as well as polymer block responses to the ternary solvent mixture. With progressing dialysis, DMAc is replaced by acetone/propan-2-ol, affecting the solubility of S/M corona patches. This induces the collapse into S patches and determines the onset of aggregation. Time-dependent ^{1}H-NMR measurements were performed by drawing samples at specific intervals during dialysis to determine the solvent composition. **b**, TEM series exemplifying the timeline of aggregation on s-**SB**$^{M(l)}$ and **SD**^{M}**S**. Up to 30 min, S corona collapses to form S patches, yet both CBBs are still stable due to stabilizing corona; after 30 min, **SD**^{M}**S** (smaller M corona) aggregate; after 45 min, aggregation of **SD**^{M}**S** proceeds, while s-**SB**$^{M(l)}$ is still stable (larger M corona, no co-assembly); at 60 min, s-**SB**$^{M(l)}$ aggregates and co-assembly takes place; up to 90 min, co-assembly is complete. (OsO_4 staining: S grey, B dark grey dots, D black, and M not visible as a result of degradation by the electron beam.)

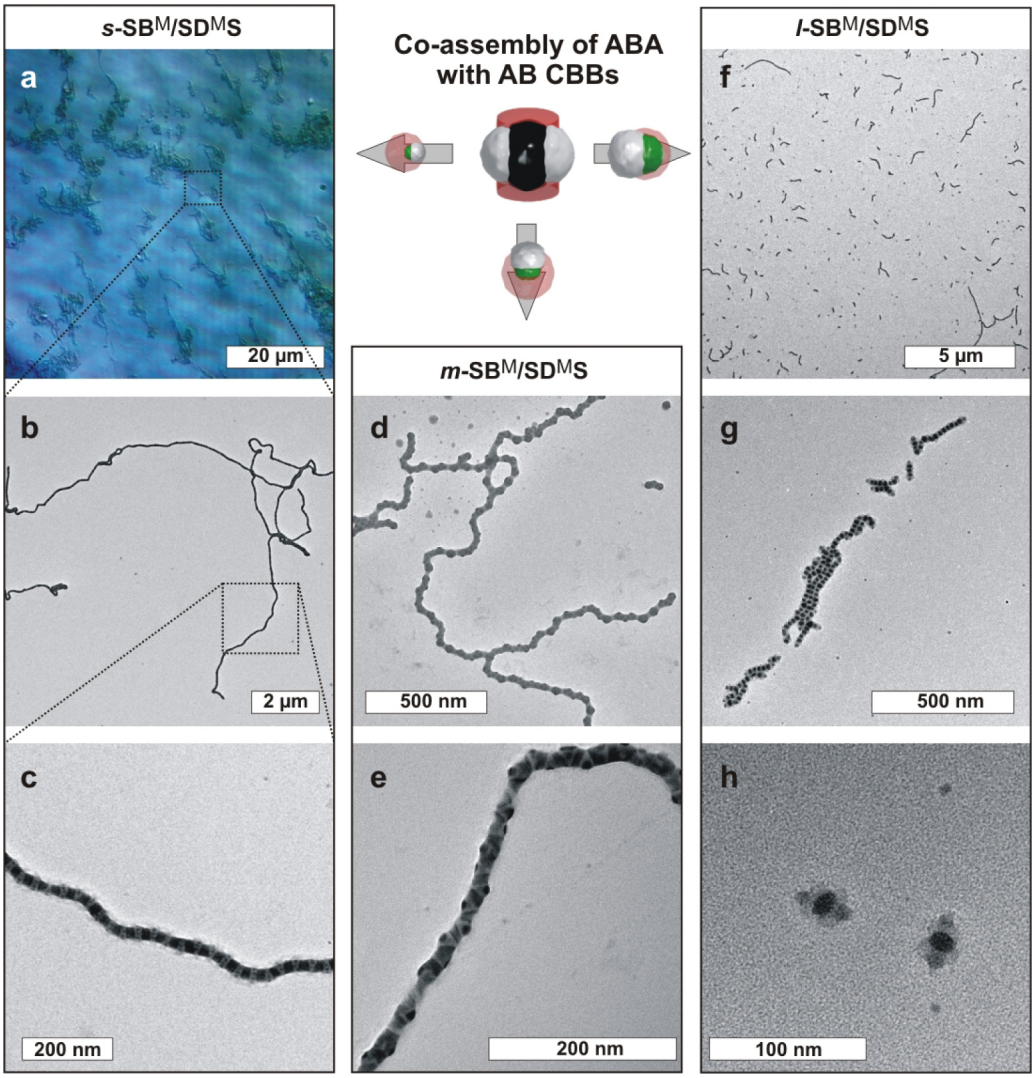

Extended Data Figure 6 | Supporting images of colloidal co-assemblies composed of SD^{M}S and s-SB^{M}, m-SB^{M} and l-SB^{M}. **a**, Optical microscopy image of colloidal co-assemblies 30 µm in length. **b**, **c**, TEM images of fully decorated –S– segments with s-**SB**^{M}. **d**, **e**, Larger m-**SB**^{M} units induce kinks due to lateral, alternating decoration and high volume displacement within the –S– segments. **f**, Zoom-out of rod-like colloidal oligomers end-capped with l-**SB**^{M}. **g**, Magnification of **f**. **h**, The smallest possible co-assembly with [**SD**^{M}**S**]$_1$; that is, two end-caps attached to one **SD**^{M}**S** unit. (OsO_4 staining: S grey, B dark grey dots, D black, and M not visible as a result of degradation by the electron beam.)

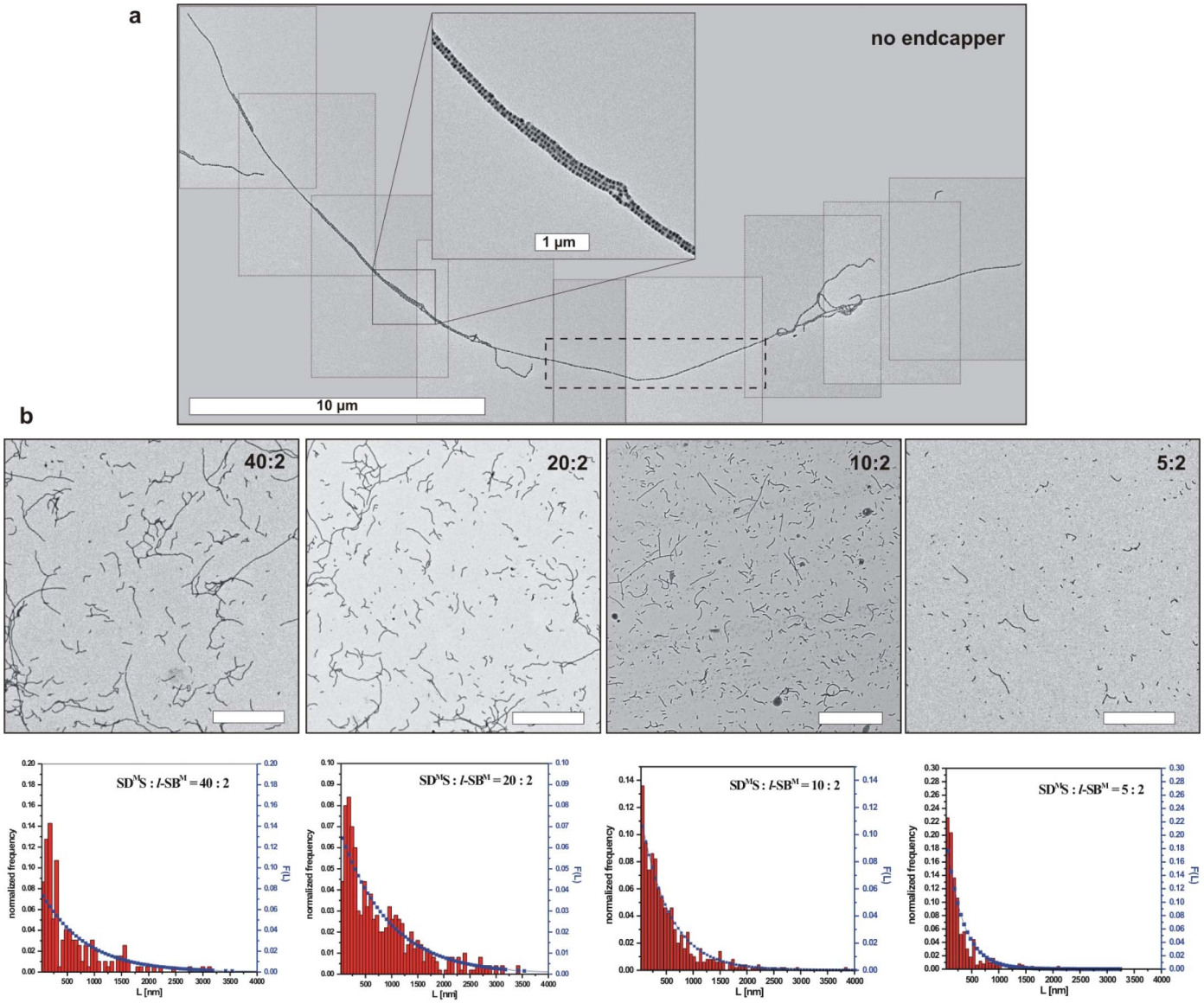

Extended Data Figure 7 | Length control of colloidal polymers via end-capping with l-SB^{M}. **a**, Without any l-**SB**^{M} end-capper added, the **SD**^{M}**S** units grow into remarkably extended superstructures several micrometres in length, exceeding 500–600 **SD**^{M}**S** repeating units. The inset illustrates the segmented core and some occurrence of branching. The displayed image consists of an overlay of nine separate TEM images, because the superstructure was far too large for magnifications that were still able to resolve the nanostructure. The dashed box marks the part of the colloidal polymer that is shown in Fig. 3d. **b**, TEM images and frequency distributions (red bars) of 500 evaluated colloidal polymers for varying **SD**^{M}**S** to l-**SB**^{M} mixing ratios of 40:2, 20:2, 10:2 and 5:2. Scale bars, 5 µm. We count segments and multiply the resulting average value by the average segment length, $L_n = 55$ nm, to yield the average length of the co-assembly. Data are plotted against the normalized frequency and fitted by a Schulz–Flory frequency distribution (squares), $F(L) = \exp(-L/L_n)/L_n$, showing a continuous decrease in the average length coinciding with the mixing ratio. The similar timescales of onset of aggregation combined with matching sizes of CBBs both promote efficient end-capping.

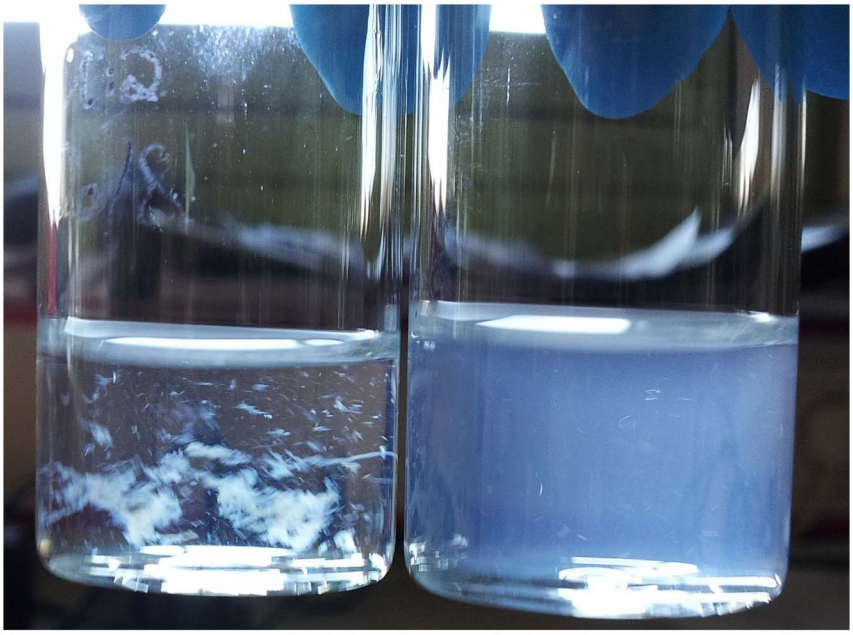

Extended Data Figure 8 | Stability of $[SD^{M}S]_m$ colloidal polymer versus $SB^{T}/[SD^{M}S]_m$ co-assembly in polar solvents. Photograph of two colloidal solutions after dialysis into ethanol. Left: instant precipitation of the $[SD^{M}S]_m$ colloidal homopolymer as a result of complete collapse of the M corona. Right: the $SB^{T}/[SD^{M}S]_m$ colloidal co-assembly is stabilized by the soluble T corona patches. Precipitation is not observed even after weeks.

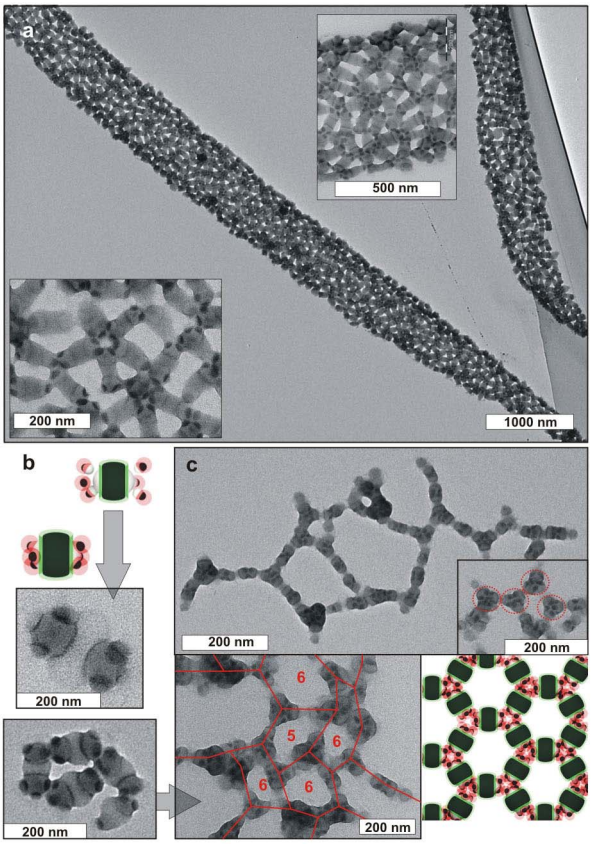

Extended Data Figure 9 | Colloidal molecules and two-dimensional network formation. **a**, Co-assembly of four **SB**^{M} with one **SD**^{T}**S** CBB by means of collapsing S patches in acetone/propan-2-ol (60:40 v/v) yields colloidal molecules with one or two end-caps of the $(SB^{M})_2$-$(SD^{T}S)$-$(SB^{M})_2$ type, permitting three or four nearest neighbours at every linking point in large-area networks. **b**, Co-assembly of six **SB**^{M} with one **SD**^{T}**S** CBB by means of collapsing S patches in acetone/propan-2-ol (60:40 v/v) yields colloidal molecules of the $(SB^{M})_3$-$(SD^{T}S)$-$(SB^{M})_3$ type. **c**, Addition of propan-2-ol until acetone/propan-2-ol reached 20:80 (v/v) selectively collapses the terminal M corona, allowing two nearest neighbours at every linking point of the network in solution. On some occasions the network takes on the form of a distorted kagome lattice.

Extended Data Table 1 | Characteristics of triblock terpolymers and CBBs

CBB Code*	Triblock Terpolymer†	$\frac{V_A}{V_B}$ ‡	$r_C = \frac{V_C}{V_A + V_B}$ ‡	d_{CBB}§ [nm]	$R_{B\text{-core}}$‖ [nm]	V_B¶ [x10³ nm³]	N_{agg}#	V_S☆ [x10³ nm³]
AB^{C}A CBBs								
SD^{M}S	$S_{560}D_{580}M_{540}^{195}$	0.37	0.33	55x24	55x30	71.2	370	26.3
SD^{T}S	$S_{510}D_{540}T_{460}^{258}$	0.36	0.44	60x30	57x38	96.1	385	34.6
SB^{M}S	$S_{590}B_{2700}M_{560}^{265}$	0.38	0.25	100x31	100x50	394.0	2300	149.7
s-AB$^{C(y)}$ CBBs of similar size, yet decreasing corona length (l), (m), (s)								
s-SB$^{M(l)}$	$S_{310}B_{150}M_{340}^{74}$	3.57	0.74	19	5 ± 2	0.5	40	1.9
s-SB$^{M(m)}$	$S_{510}B_{260}M_{260}^{90}$	4.20	0.34	28	7 ± 2	1.4	60	5.9
s-SB$^{M(s)}$	$S_{700}B_{270}M_{180}^{105}$	4.50	0.15	29	7 ± 2	1.4	57	6.3
***x*-AB^C CBBs of different overall size s-, m-, l-.**								
s-SB^M	$S_{310}B_{150}M_{340}^{74}$	3.57	0.74	19	5 ± 2	0.5	40	1.9
m-SB^M	$S_{560}B_{580}M_{540}^{143}$	1.78	0.88	35	11 ± 2	5.6	140	9.9
l-SB^M	$S_{610}B_{640}M_{290}^{140}$	1.72	0.26	47	15 ± 2	14.1	260	24.3
AB CBBs with different nature of the corona								
SB^T	$S_{510}B_{540}T_{480}^{155}$	1.70	0.45	28	9 ± 2	3.1	60	5.2
SB^V	$S_{360}B_{380}V_{590}^{120}$	1.67	0.95	22	7 ± 2	1.4	54	2.4

* The syntheses and characterization of SBM, SBV and SBT triblock terpolymers were reported in detail previously[31–35]. Superscripts denote the size of the soluble corona patches in relation to the other CBBs: s, small; m, medium; l, large.

† Subscripts denote the degrees of polymerization of the corresponding blocks, and the superscript is the molecular mass in kg mol^{-1} determined with combined ^{1}H-NMR and GPC (polydispersity index < 1.15) measurements.

‡ Volume fractions V_A, V_B and V_C were calculated from molar volumes and degrees of polymerization.

§ For calculations see Methods. The diameter (d) and width (w) of cylindrical segments of **AB^{C}A** units and (**AB^{C}A**)$_x$ segments are average values from TEM image analysis.

‖ Average of 250 measured particle core radii in TEM image analysis.

¶ Particle core volumes calculated from measured core radii.

Average aggregation number of polymer chains per particle.

☆ Calculated by applying the relation V_S/V_B.